Central European Journal of Energetic Materials, **2014**, *11*(3), 335-348
ISSN 2353-1843

Study on the Initiation Capacities of Conical Ring Booster Pellets

Lishuang HU[1*], Shuangqi HU[1], Xiong CAO[1], Juanjuan LI[2]

[1]*Chemical Industry and Ecology College,*
North University of China, Taiyuan, Shanxi 030051, P.R. China
[2]*Jinxi industries group Co., Ltd,*
Taiyuan, Shanxi 030051, P.R. China
[*]*E-mail: hlsly1314@163.com*

Abstract: The insensitive main charge explosive is becoming an important part of modern weapon development. Insensitive main charge explosives generally have a high critical initiation pressure. The detonation pressure of a traditional cylindrical booster pellet is constant at a specific density and consequently has insufficient energy output to reliably initiate an insensitive main charge explosive. To ensure that this requirement could be achieved, the conical ring booster pellet was designed and optimized. Eight-point-synchronous explosive circuits were designed as appropriate to the sizes of the four booster pellets. The initiation processes of the four conical booster pellets equipped with the eight-point circuit were simulated using ANSYS/LY-DYNA software. The experimental measurements were performed in order to test the initiation capacities of these conical booster pellets. The results demonstrated that their initiation capacities are much better than the initiation capacity of a cylindrical booster pellet. The optimum size of the conical ring booster pellet is when the ratio of the inner to the upper diameter is 0.52, the ratio of the inner to the lower diameter is 0.44, and the ratio of the height to the lower diameter is 0.50.

Keywords: booster pellet, main charge, initiation capacity, numerical simulation, optimization

1 Introduction

The study of insensitive munitions is becoming the most important research topic of modern weapon development [1]. Any munition contains a booster system to

provide reliable initiation and detonation transfer. As the main explosives fillings for insensitive munitions have become increasingly insensitive to external stimuli, the size of the cylindrical booster explosive used in the explosive train has been increased [2]. This has resulted in the explosive train becoming a significant factor in overall weapon vulnerability. The development of booster explosives has therefore been aimed at new, highly effective booster charge structures of small size that will reliably initiate the main explosives.

Dallman [3] studied the initiation technology of a hemispherical booster explosive. The data showed that a main charge explosive with a large critical initiation diameter could be reliably initiated using this initiation system. Spahn [4, 5] studied an embedded can booster and an explosive ring booster. These two booster systems both have powerful output energies, sufficient to initiate main charge explosives. They are useful for initiating insensitive main charge explosives with large critical initiation pressures. We have studied the initiation capacities of ring and conical ring booster pellets in conjunction with multi-point-synchronous explosive circuits in a recent paper [6]. The initiation capacity of a conical ring booster pellet is much better than that of a ring booster pellet with the same mass and density. However, the number of studies on booster pellet structures is limited.

In the present paper, conical ring booster pellets were optimized for four different sizes. These four conical ring booster pellets were investigated by numerical simulation and experimental measurement.

2 Numerical Simulation

Conical ring booster pellets of four different sizes are shown in Figure 1. The initiation capacity of the conical ring booster pellet of Figure 1(a) was studied previously [6]. The other three were designed on the same basis as Figure 1(a), but maintaining the same volume.

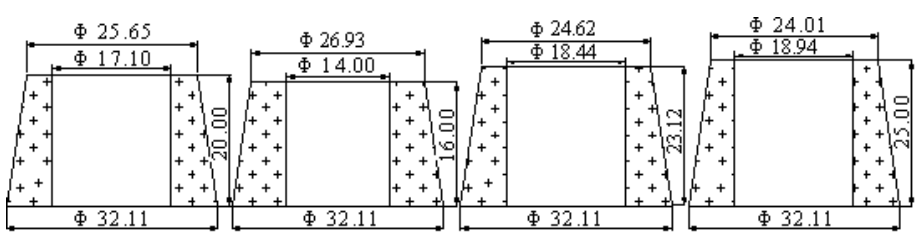

(a) (b) (c) (d)

Figure 1. The shapes and dimensions of the conical ring booster pellets.

The volume of conical ring booster pellet (a) is:

$$V = \pi \times (\frac{1}{12} \times 32.11^2 \times 99.412 - \frac{1}{12} \times 25.65^2 \times 79.412 - \frac{1}{4} \times 17.10^2 \times 20.00)$$

$= 8562.8\ mm^3 = 8.563\ cm^3$

The volumes of the booster pellets (b), (c) and (d) are all 8.563 cm^3.

2.1 Calculation model and element algorithm

ANSYS/LS-DYNA software using the LS-DYNA explicit finite element program was used. The calculation models of the conical ring booster pellets are shown in Figure 2.

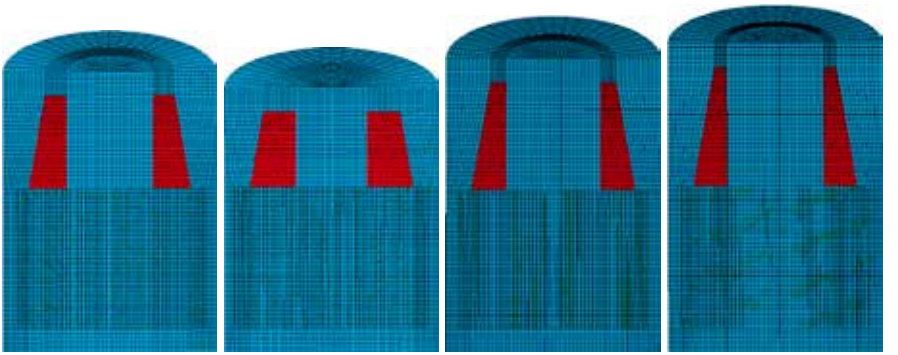

(a) (b) (c) (d)

Figure 2. The finite mesh models.

The quarter-symmetry model was adopted to establish the finite element model under eight-point initiation on the top. The Arbitrary-Lagrangian-Eulerian (ALE) method was employed for the charge and air, whereas the Lagrange algorithm was utilized for the steel witness plate. The solid-fluid interaction algorithm was used for the charge, air, and steel witness plate.

2.2 Material models

The booster explosive used in this setup was PBXN-5. The pressure for the detonation products from the PBXN-5 explosive was calculated by using the Jones-Wilkins-Lee (JWL) equation of state [7]. The equation of state has the following expression:

$$p = A\left(1-\frac{\omega}{R_1V}\right)e^{-R_1V} + B\left(1-\frac{\omega}{R_2V}\right)e^{-R_2V} + \frac{\omega E}{V} \tag{1}$$

where: p is the pressure; A, B, R_1, R_2, and ω are coefficients fitted by experiment; V is the relative volume and E is the specific internal energy. The parameters of PBXN-5 are shown in Table 1.

Table 1. Parameters of PBXN-5

Parameters of C-J			Parameters of the JWL equation of state					
ρ [g/cm^3]	p [Gpa]	D [m/s]	A [Gpa]	B [Gpa]	R_1	R_2	ω	E_0 [Gpa]
1.68	26	8100	805	18	4.60	1.30	0.38	10

The medium in which the shock wave propagated was air. The air was modeled by the linear-polynomial equation of state [8]. The equation of state is:

$$P = C_0 + C_1\mu + C_2\mu^2 + C_3\mu^3 + (C_4 + C_5\mu + C_6\mu^2)E \tag{2}$$

where: C_0, C_1, C_2, C_3, C_4, C_5 and C_6 are constants. For air, C_0=C_1=C_2=C_3=C_6=0, and C_4=C_5= γ-1, with γ the ratio of specific heats. $\mu = 1/V - 1$, where V is the relative volume. E is the specific internal energy. Therefore, for air equation (2) reduces to:

$$P = (\gamma - 1)\frac{1}{V}E \tag{3}$$

The steel witness plate was 1045 steel. The Johnson-Cook model [9], which accounts for the effects of strain hardening and strain-rate hardening, and the Gruneisen equation of state [10] were adopted to describe the dynamic response of the steel. The Gruneisen equation of state defines the pressure for compressed materials as:

$$p = \frac{\rho_0 C^2 \mu[1 + (1-\frac{\gamma_0}{2})\mu - \frac{a}{2}\mu^2]}{[1-(S_1-1)\mu - S_2\frac{\mu^2}{\mu+1} - S_3\frac{\mu^3}{(\mu+1)^2}]^2} + (\gamma_0 + a\mu)E \tag{4}$$

Where: γ_0 is the Gruneisen gamma; a is the first order volume correction to γ_0; S_1, S_2, and S_3 are the coefficients of the slope of the v_s-v_p curve; C is the intercept of the v_s-v_p curve; $\mu = 1/V - 1$

2.3 Numerical simulation results and discussion

2.3.1 Numerical simulation results for booster pellet (a)

The results of the axial initiation process are shown in Figure 3.

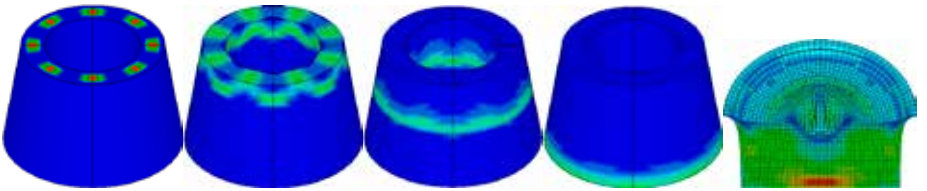

(a) t = 0.1974 μs (b) t = 0.5872 μs (c) t = 1.2905 μs (d) t = 2.4958 μs (e) t = 23.6910 μs

Figure 3. Axial initiation process of booster pellet (a).

From Figure 3, the specific initiation process of booster pellet (a) can be observed. At t = 0.5872 μs, two adjacent detonation waves show oblique impacts, and the peak value of the pressure increases. At t = 1.2905 μs, the shape of the wave front is smooth. At t = 2.4958 μs, the front of the detonation wave reaches the bottom of the charge, and the wave front is quite smooth. The process of shock wave penetration into the steel witness plate terminates at t = 23.6910 μs. A dent depth of 10.45 mm is produced in the steel witness plate.

The results of the radial convergence process are shown in Figure 4.

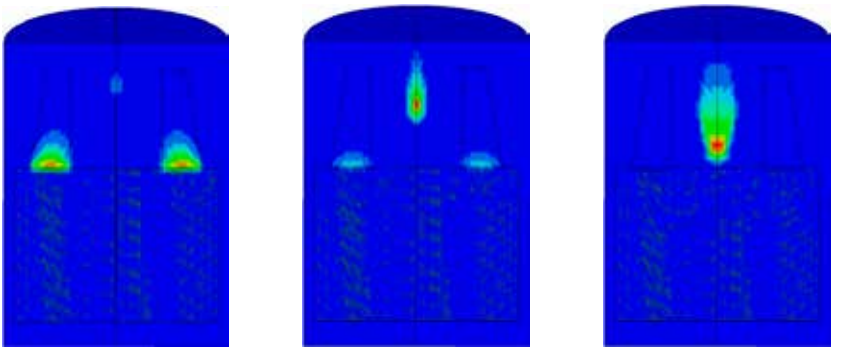

(a) t = 2. 5958 μs (b) t = 3.0926 μs (c) t = 3.9989 μs

Figure 4. Radial convergence process of booster pellet (a).

When booster pellet (a) is simultaneously initiated at eight symmetrical points, the detonation wave propagates in the axial direction and also along the radial direction of the pellet at the same time. When the detonation wave reaches the internal surface of the booster pellet, it will attenuate into the shock

wave in the central air medium and propagate to the central axis of the pellet. The shock wave propagating to the central axis of the booster pellet is gradually strengthened. At $t = 2.5958$ μs, the shock wave propagating to the center of the booster pellet begins to converge, and the pressure gradually increases. At that time, the detonation wave basically reaches the bottom of the booster pellet in the axial direction. Because the speed of the shock wave propagating in the center of the booster pellet is slower, the center convergence time has a certain time delay relative to the axial detonation. At $t = 3.0926$ μs, the central convergence pressure reaches a maximum of $p = 34.01$ Gpa.

2.3.2 Numerical simulation results for booster pellet (b)

The results of the axial initiation process are shown in Figure 5, and the results of the radial convergence process are shown in Figure 6.

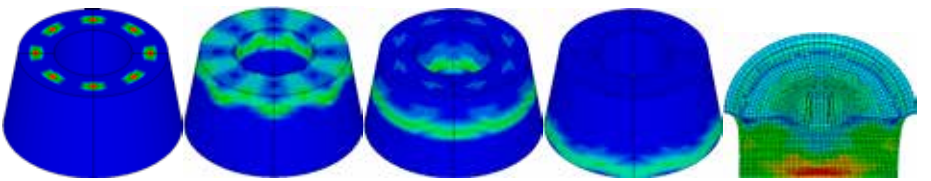

(a) $t = 0.1901$ μs (b) $t = 0.5782$ μs (c) $t = 1.0918$ μs (d) $t = 2.0910$ μs (e) $t = 23.0980$ μs

Figure 5. Axial initiation process of booster pellet (b).

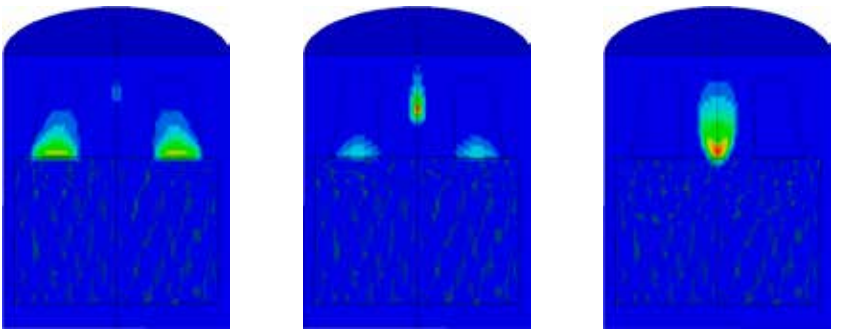

(a) $t = 2.1948$ μs (b) $t = 2.5913$ μs (c) $t = 3.3980$ μs

Figure 6. Radial convergence process of booster pellet (b).

The axial initiation process and the radial convergence process of booster pellet (b) are similar to those of booster pellet (a). However, the peak pressure is 36.21 Gpa, and the dent depth is 10.86 mm.

2.3.3 Numerical simulation results for booster pellet (c)

The results of the axial initiation process are shown in Figure 7, and the results of the radial convergence process are shown in Figure 8.

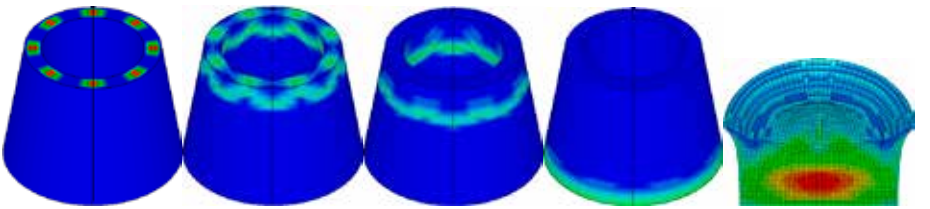

(a) t = 0.1944 μs (b) t = 0.5969 μs (c) t = 1.3481 μs (d) t = 2.8871 μs (e) t = 24.4325 μs

Figure 7. Axial initiation process of booster pellet (c).

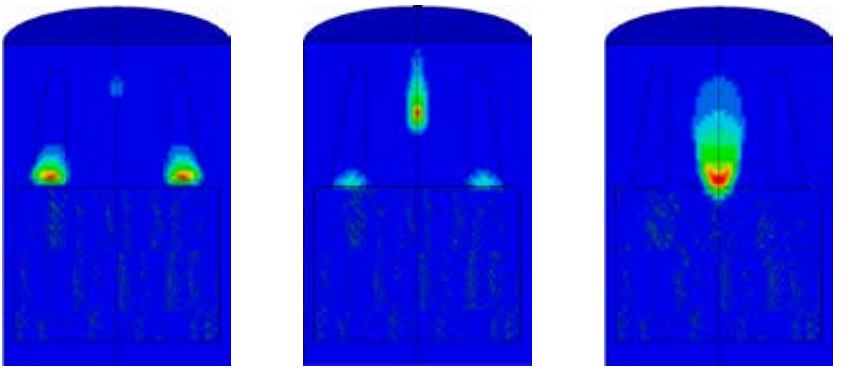

(a) t = 2. 7917 μs (b) t = 3.3894 μs (c) t = 4.3984 μs

Figure 8. Radial convergence process of booster pellet (c).

The axial initiation process and the radial convergence process of booster pellet (c) are similar to those of booster pellet (a). The maximum pressure is 33.23 Gpa, and the dent depth is 9.88 mm.

2.3.4 Numerical simulation results for booster pellet (d)

The results of the axial initiation process are shown in Figure 9, and the results of the radial convergence process are shown in Figure 10.

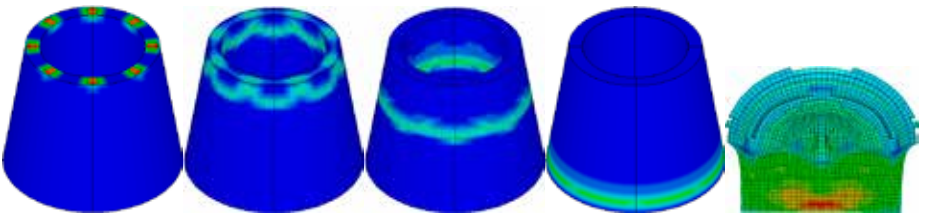

(a) t = 0.1966 μs (b) t = 0.5992 μs (c) t = 1.3994 μs (d) t = 3.0892 μs (e) t = 24.9940 μs

Figure 9. Axial initiation process of booster pellet (d).

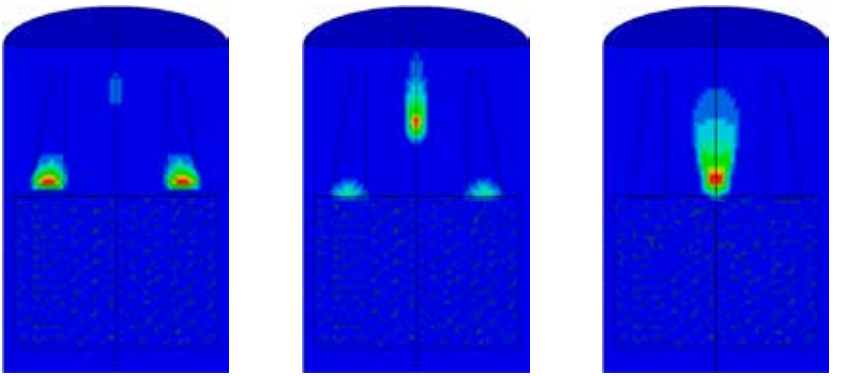

(a) t = 2. 8979 μs (b) t = 3.5897 μs (c) t = 4.7999 μs

Figure 10. Radial convergence process of booster pellet (d).

The axial initiation process and the radial convergence process of booster pellet (d) are similar to those of booster pellet (a). The maximum pressure is 31.64 Gpa, and the dent depth is 9.47 mm.

The simulation results are presented in Table 2.

Table 2. Simulation results

Booster pellet	Simulation maximum pressure [Gpa]	Simulation dent depth [mm]
Booster pellet (a)	34.01	10.45
Booster pellet (b)	36.21	10.86
Booster pellet (c)	33.23	9.88
Booster pellet (d)	31.64	9.47

The simulation results show that the initiation capacity of booster pellet (b) is the best. The maximum difference between the convergence pressures of the four conical booster pellets is 4.57 Gpa, but the maximum difference between the depths is 1.39 mm. According to the critical initiation energy criterion

formula $p^2\tau = c$ [11], the initiation capacity is affected by both the pressure and the action time. The convergence pressure of booster pellet (b) is the largest, but the action time is the shortest. The convergence pressure of booster pellet (d) is the smallest, but the action time is the longest. Consequently the depths from these two booster pellets show little difference.

3 Experimental

3.1 Experimental method

Main charge axial-steel-dent and pressure test methods were used in this work. The first method has been explained in Ref. [6]. In the pressure test method, a manganin piezoresistive sensor was used to measure the convergence pressure.

In these experiments, a low resistance manganin piezoresistive sensor was used to measure the convergence pressure more accurately. The pressure can be calculated by the following formula:

$$p = \begin{cases} 1.978 + 35.28\dfrac{\Delta R}{R} & (>5.907 \quad Gpa) \\ 53.22\dfrac{\Delta R}{R} & (0 \sim 5.907 \quad Gpa) \end{cases} \tag{5}$$

The formula was obtained through calibration of the manganin piezoresistive sensor at the Beijing Institute of Technology.

In the experiments, we used a constant current source to measure $\Delta U/U$ by oscillography, and then $\Delta R/R$ was obtained according to the following formula:

$$\frac{\Delta U}{U} = \frac{\Delta RI}{RI} = \frac{\Delta R}{R} \tag{6}$$

3.2 Experimental conditions

3.2.1 Selection of the booster explosive

The booster explosive PBXN-5 was used in these experiments. The pressed-explosive densities of the booster pellets were all 1.68 g/cm^3. The diameter and density of the cylindrical booster pellets were 29.58 mm and 1.68 g/cm^3, respectively. The conical ring booster pellets are shown in Figure 11.

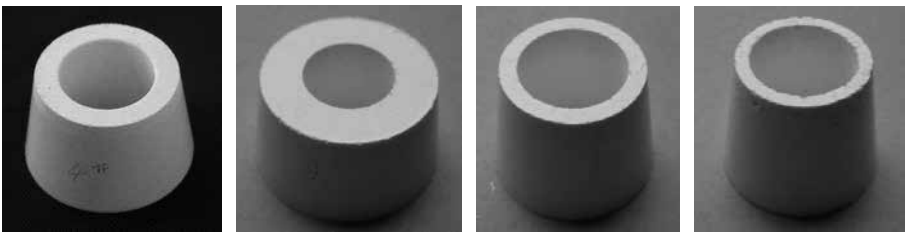

(a) (b) (c) (d)

Figure 11. Conical ring booster pellets.

3.2.2 Preparation of the eight-point-synchronous explosive circuits

The eight-point-synchronous explosive circuits contain base plates and cover plates. Ultra-fine HMX was selected as the circuit charge. The charge densities of the eight-point-synchronous explosive circuits were 1.36~1.37 g/cm^3. The base plate is shown in Figure 12 and the cover plate in Figure 13.

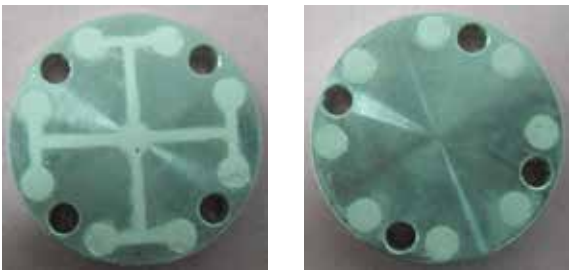

(a) Front side (b) Back side

Figure 12. Base plate.

Figure 13. Cover plate.

3.2.3 Selection of the main charge explosive

The pressed TNT was chosen as the main charge explosive. The density, diameter and height of the TNT charges were 1.51 g/cm^3, 50.0 and 22.0 mm respectively.

3.2.4 Selection of the steel witness plate

The steel witness plate was a general carbon steel of size Φ100×50 mm.

3.3 Experimental devices

The testing device for the convergence pressure is illustrated in Figure 14. The experimental device for the main charge axial-steel-dent method is shown in Figure 15.

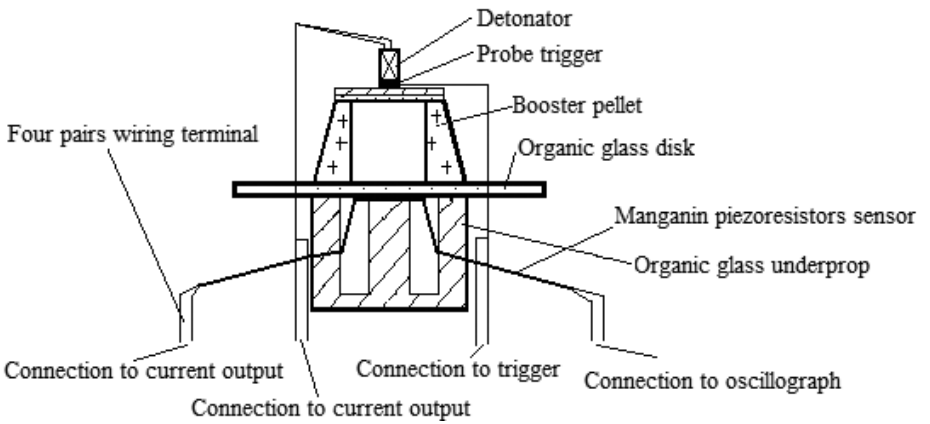

Figure 14. Diagrammatic illustration of the pressure test method.

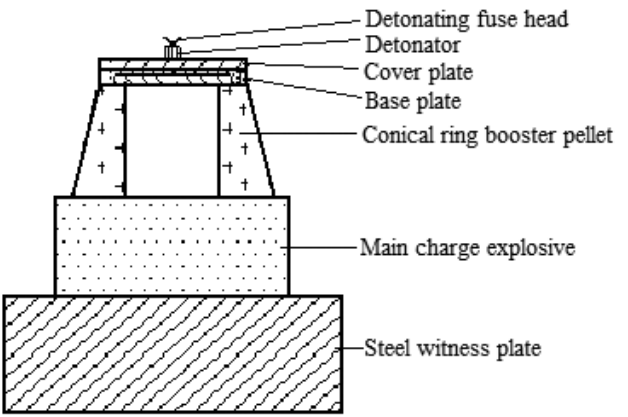

Figure 15. Device for the main charge axial-steel-dent method.

3.4 Experimental results and discussion

The experimental results are shown in Table 3.

Table 3. Results of the initiation capacities of cylindrical and conical ring booster pellets

Shape	Mass [g]	Average value of dent data [mm]	Convergence pressure [Gpa]
Cylindrical	19.7	2.80	26.0
Cylindrical	22.4	3.10	26.0
Cylindrical	26.7	3.28	26.0
Cylindrical	33.1	3.56	26.0
Booster pellet (a)	14.4	3.29	31.1
Booster pellet (b)	14.4	3.48	32.4
Booster pellet (c)	14.4	3.06	30.2
Booster pellet (d)	14.4	2.92	29.6

The steel dent data for the four conical ring booster pellets are larger than those of the cylindrical booster pellets. The convergence pressures of the four conical ring booster pellets are 31.1, 32.4, 30.2 and 29.6 Gpa, respectively. They are all larger than the convergence pressure 26.0 Gpa of the cylindrical booster pellet. The conical ring booster pellets can use less explosive mass than ordinary cylindrical booster pellets to generate the same dent data. The experimental results are in good agreement with the numerical simulation ones. Under these experimental conditions, the optimum size of the conical ring booster pellet is with a ratio of the inner to the upper diameter of 0.52, a ratio of the inner to the lower diameter of 0.44, and a ratio of the height to the lower diameter of 0.50.

The effect of the conical ring booster pellet on the main charge explosive consists of two parts. One is the detonation wave pressure produced by the booster pellet in the axial direction. The other is the shock wave convergence pressure from the booster pellet in the radial direction. The shock wave convergence effect is dominant. That is why conical ring booster pellets have a greater initiation capacity.

According to reference [12], the shock wave overpressure decreases with increased distance. They have the following correlation:

$$\Delta p = f(\frac{\sqrt[3]{m}}{h}) \tag{7}$$

where m is the TNT explosive equivalence, and h is the shock wave

propagation distance.

The shock wave propagation distance of booster pellet (b) is the shortest and the effective charge effect on the shock wave convergence is the largest. Therefore, the initiation capacity of booster pellet (b) is the best.

4 Conclusions

The initiation capacities of four conical ring booster pellets were studied by numerical simulation and experimental measurement. Several conclusions have been made:

- The initiation capacity of a conical ring booster pellet is more powerful than that of a cylindrical booster pellet with the same mass and density.
- The convergence pressure of a conical ring booster pellet is much higher than that of a cylindrical booster pellet with the same density.
- The results have been validated by both numerical simulation and experimental measurement.

5 References

[1] *Department of Defense Test Method Standard: Hazard Assessment Tests for Non-Nuclear Munitions*, MIL-STD-2105B, Department of Defense, **1994**.

[2] Flegg G.T., Frankl P.J., Griffiths T.T., *Explosive Train Scale Shock Testing of New Energetic Materials*, QinetiQ, Fort Halstead, Sevenoaks, Kent, TN14 7BP, UK, **2010**.

[3] Dallman J.C., *Measurements of Detonation-Wave Spreading and Local Particle Velocity at the Surface of 17-mm LX-07 Hemispherical Boosters*, Report No. LA-11414-MS, Los Alamos National Laboratory, **1988**.

[4] Spahn P.F., *Booster Explosive Ring*, US Patent 5233929, **1993**.

[5] Spahn P.F., *Embedded Can Booster*, US Patent 5221810, **1993**.

[6] Hu L.S., Hu S.Q., Cao X., Study on the Initiation Capacities of Two Booster Pellets, *Cent. Eur. J. Energ. Mater.*, **2012**, *9*(3), 261-272.

[7] Lee E.L., Hornig H.C., Kury J.W., *Adiabatic Expansion of High Explosive Detonation Products*, Report No. UCRL-50422, Lawrence Livermore National Laboratory, Livermore, CA, **1968**.

[8] Alia A., Souli M., High Explosive Simulation Using Multi-Material Formulations, *Appl. Therm. Eng.*, **2006**, *26*(10), 1032-1042.

[9] Johnson G.R., Cook W.H., Fracture Characteristics of Three Metals Subjected to Various Strains, Strain Rates, Temperatures and Pressures, *Eng. Fract. Mech.*, **1985**, *21*(1), 31-48.

[10] Li Y., *Experiment of Booster Shock Initiation and Its Numerical Simulation* (in Chinese), North University of China, China, **2010**.
[11] Walker F.E., Wasley R.J., Critical Energy for Shock Initiation of Heterogeneous Explosives, *Explosivstoffe*, **1969**, *17*(1), 9-13.
[12] Zhang S.Z., *Explosion Principle* (in Chinese), National Defense Industry Press, Beijing, **2005**, pp. 394-397.